Experimental study of photonic crystals consisting of ϵ-negative and μ-negative materials

Liwei Zhang,[1] Yewen Zhang,[1,2,*] Li He,[1] Hongqing Li,[1,2] and Hong Chen[1,2]
[1]*Pohl Institute of Solid State Physics, Tongji University, Shanghai 200092, People's Republic of China*
[2]*School of Electronics and Information, Tongji University, Shanghai 200092, People's Republic of China*
(Received 18 July 2006; revised manuscript received 8 October 2006; published 30 November 2006)

ϵ-negative (ENG) and μ-negative (MNG) materials are successfully fabricated by using composite right/left-handed transmission line. The ENG and MNG materials are opaque in experiments, but the completely tunneling phenomenon occurs in the ENG-MNG pair, if the wave impedance and the effective phase shift of ENG and MNG materials are under the conditions of match, respectively. We experimentally confirmed that the photonic crystals consisting of ENG and MNG materials can possess left-handed propagation modes and right-handed propagation modes within forbidden gaps. At the same time, the Bragg gaps for the band-gap indices $m=\pm 1$ and the zero effective phase (zero-Φ_{eff}) gaps were also observed. The experimental results agree extremely well with the simulations.

DOI: 10.1103/PhysRevE.74.056615 PACS number(s): 42.70.Qs, 78.20.Ci, 41.20.Jb

I. INTRODUCTION

The electromagnetic (EM) properties of a material can be described by its corresponding electric permittivity (ϵ) and magnetic permeability (μ). These two parameters macroscopically describe the effects of induced electric and magnetic polarization. A medium can transmit electromagnetic waves in it when both ϵ and μ have the same sign, i.e., either negative or positive. If they have opposite signs, the medium supports only evanescent wave but effectively reflects the incoming electromagnetic wave. The metamaterial that exhibits simultaneously negative electric permittivity and magnetic permeability in a frequency band is called double negative (DNG) material or left-handed material (LHM), and was first introduced theoretically by Veselago [1]. It exhibits many unusual physical properties different from the conventional right-handed material (RHM). LHM does not exist in nature, but the artificial LHMs have been realized by using periodic structures either with the unit cell of split-ring resonators (SRR) and conducting wires [2,3] or with the unit cell of LC-loaded transmission line [4,5], in particular, the transmission line (TL) approach towards metamaterials with LH and RH attributes, known as composite right/left-handed transmission line (CRLH TL). It presents the advantage of lower losses over a broader bandwidth and has already been demonstrated in various novel component and coupler applications [6,7].

There are two types of the single negative (SNG) materials [8–10], e.g., the ϵ-negative (ENG) material with negative permittivity but positive permeability and the μ-negative (MNG) material with negative permeability but positive permittivity. Because ϵ and μ are frequency dependent, only within a certain frequency range we have ENG or MNG, which is called the SNG frequency range. Metamaterial with $\epsilon<0$ can easily be realized by periodically arranged metallic wires [11]; on the other hand, the metamaterial with $\mu<0$ can be implemented by a periodic array of metallic split-ring resonator (SRR) structures [12]. In a mismatched CRLH TL, the single negative (SNG) material can be realized between left-handed passband and right-handed passband [13]. For the SNG materials, the electromagnetic wave is evanescent, but it is surprising that the propagation mode can be formed by the interaction of the evanescent-wave-based interface modes in the photonic crystals stacked by alternating ENG and MNG materials [8,14].

The pure ENG and pure MNG materials are represented in Ref. [9] with the transmission line models by periodically loading lumped-element components, but it is difficult to verify in experiment. In this paper, SNG materials were physically fabricated using the CRLH TL by periodically loading lumped-element series capacitors (C) and shunt inductors (L). The properties of transmission are measured by the Agilent 8722ES vector network analyzer. The experimental results show that the tunneling phenomenon occurs in the ENG-MNG pair under special conditions, and the photonic crystals consisting of ENG and MNG materials can possess left-handed propagation modes and right-handed propagation modes within forbidden gaps. At the same time, the photonic gaps for the band-gap indices $m=\pm 1$ and the zero effective phase (zero-Φ_{eff}) gaps were also observed. The experimental results agree extremely well with the simulations.

II. EXPERIMENT AND SIMULATION

The proposed unit cell of the CRLH TL is shown in Fig. 1. The structure consists of a host TL medium with the dis-

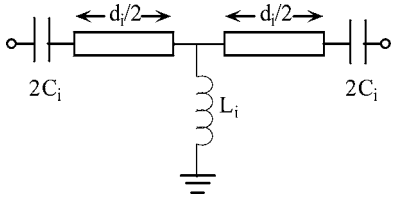

FIG. 1. The schematic and circuit model of a CRLH TL unit with the loading lumped element series capacitors (C_i) and shunt inductor (L_i).

*Author to whom correspondence should be addressed. Email address: yewenzhang@online.sh.cn

tributed parameters L_0 and C_0 periodically loaded with discrete lumped element components, L and C. When the average lattice constant d_i is much smaller than the guided wavelength λ_g, $d<\lambda_g/4$, the structure exhibits a macroscopic behavior rigorously expressed with the constitutive parameters ϵ and μ. The CRLH TL fabricated by cascading the unit cells of Fig. 1 periodically is effectively homogeneous in a certain range of frequencies [15]. The dispersion characteristics of the structure can be determined by the periodic analysis [16]; the effective relative permittivity and permeability are given by the following approximate expressions,

$$\epsilon_i \approx \left(C_0 - \frac{1}{\omega^2 L_i d_i}\right) \Big/ (\epsilon_0 p), \quad \mu_i \approx p\left(L_0 - \frac{1}{\omega^2 C_i d_i}\right) \Big/ \mu_0, \tag{1}$$

where p is a structure constant and $i=1, 2$ notes the different type of CRLH TL. The corresponding dispersion diagram of a mismatched CRLH TL unit exhibits a band structure with two distinct passbands and stopbands. Expressions for the pertinent cutoff frequency f_1 and eigenfrequencies f_2 and f_3 are as follows [6]:

$$f_1 = \frac{1}{4\pi\sqrt{L_i C_i}}, \quad f_2 = \frac{1}{2\pi\sqrt{C_0 L_i d_i}}, \quad f_3 = \frac{1}{2\pi\sqrt{L_0 C_i d_i}}, \tag{2}$$

the lower frequency range in the passband is left handed (LH), the upper frequency range is right handed (RH), and the stopband displaying between f_2 and f_3 is either ENG or MNG in nature, depending on the CRLH TL parameters. For the sake of simplicity, the CRLH TLs which possess ENG or MNG in a certain range of frequencies are termed ENG TL and MNG TL, respectively. For the ENG TL, the eigenfrequency $f_2>f_3$, while for MNG TL, the eigenfrequency $f_2<f_3$.

ENG TL and MNG TL have been made by FR-4 substrate with a thickness of $h=1.6$ mm, relative permittivity of $\epsilon_r=4.75$, and relative permeability $\mu_r=1.0$. In order to manufacture the ENG TL, 50 Ω TLs were designed to have a length of $d_1=7.2$ mm, the loading lumped-element components $L_1=5.6$ nH, $C_1=5.1$ pF, and in the MNG TL, $d_2=8.4$ mm, the loading lumped elements $L_2=10$ nH and $C_2=2$ pF, respectively. As for the actual microstrip line, the effective relative permittivity ϵ_{re} of the microstrip line is dependent on the substrate thickness h, substrate relative permittivity ϵ_r, and conductor width w,

$$\epsilon_{re} = \frac{\epsilon_r + 1}{2} + \frac{\epsilon_r - 1}{2}\left(1 + \frac{12h}{w}\right)^{-1/2} \approx 3.57$$

(for $w/h \geq 1$). As a result of the characteristic impedance of the microstrip line $Z_0=\sqrt{\mu_0/(\epsilon_0\epsilon_{re})}/p$ [17], then $p\approx 4.05$ for our transmission line. From about 0.56 GHz to 5.5 GHz, ENG TL and MNG TL are effectively homogeneous media with different permittivity and permeability. According to Eq. (1), the relative permittivity and permeability of the ENG TL and MNG TL can be calculated as shown in Figs. 2(a) and 2(b), respectively. It is shown clearly that the frequency range, where $\epsilon<0$ and $\mu>0$, for ENG TL is 1.45–2.2 GHz, and the frequency range, where $\mu<0$ and $\epsilon>0$, for MNG TL is 1.53–2.2 GHz.

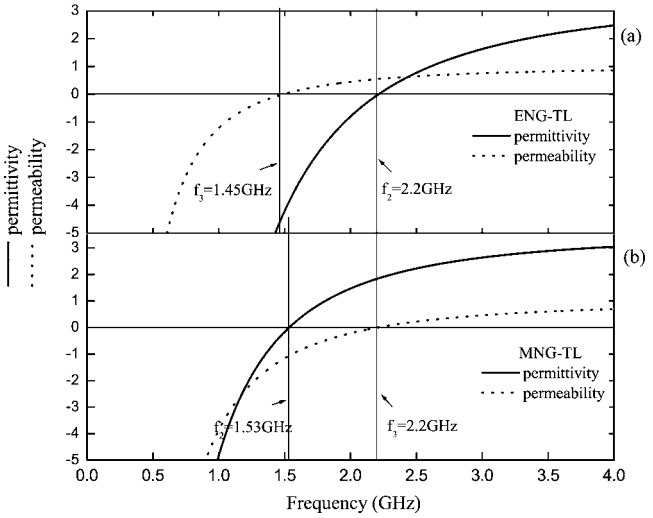

FIG. 2. The calculated relative permittivity (ϵ) and permeability (μ) of the ENG TL (a) with series capacitor $C=5.1$ pF, shunt inductor $L=5.6$ nH, where the eigenfrequency $f_2>f_3$ and MNG TL (b) with series capacitor $C=2$ pF, shunt inductor $L=10$ nH, where the eigenfrequency $f_2<f_3$ using ideal lumped element components, respectively.

Figures 3(a) and 3(b) depict the simulated and measured S parameters of ENG TL and MNG TL containing twelve CRLH TL units, respectively. The cutoff frequency and eigenfrequencies of the simulated results are about 0.42 GHz, 1.28 GHz, and 2.03 GHz for ENG TL, and 0.51 GHz, 1.28 GHz, and 2.08 GHz for MNG TL, respectively. They move a little to lower frequency in comparison with the calculated values shown in Fig. 2, because we simulated the S parameters using real lumped element components. For the simulation and measurement, they agree well

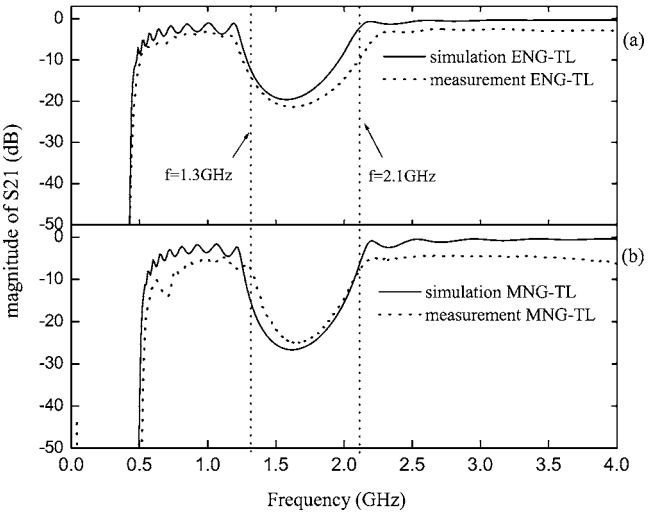

FIG. 3. The simulated and measured S parameters of proposed ENG TL (a) with series capacitor $C=5.1$ pF, shunt inductor $L=5.6$ nH and MNG TL (b) with series capacitor $C=2$ pF, shunt inductor $L=10$ nH using real lumped element components, respectively.

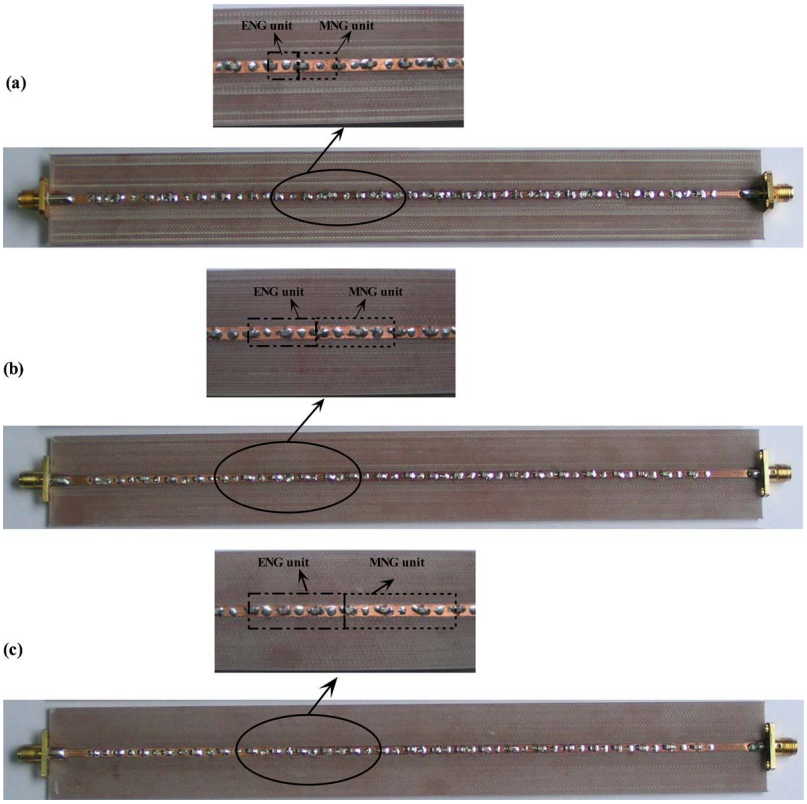

FIG. 4. (Color online) Photograph of the fabricated photonic crystals $(ENG_1MNG_1)_{12}$ (a), $(ENG_2MNG_2)_6$ (b), and $(ENG_3MNG_3)_4$ (c), based on CRLH TLs, respectively.

with each other. By and large, ENG TL and MNG TL are all SNG materials over the frequencies 1.3 GHz–2.1 GHz in our experiments.

Effective LHM can be formed by having alternating ENG layers and MNG layers, which have been investigated by Fredkin and Ron in theory [8]. To demonstrate the LH transmission characters of the periodic structures cascaded ENG materials with MNG materials in experiment, we fabricated three kinds of one-dimensional photonic crystals with $(ENG_1MNG_1)_{12}$, $(ENG_2MNG_2)_6$, and $(ENG_3MNG_3)_4$, where the subscripts "1," "2," and "3" represent the number of ENG TL and MNG TL units in one period, and "12," "6," and "4" represent the period, respectively. The photograph of the fabricated photonic crystals $(ENG_1MNG_1)_{12}$, $(ENG_2MNG_2)_6$, and $(ENG_3MNG_3)_4$ are shown in Fig. 4.

Figure 5(a) shows the advanced design systems (ADS) of agilent simulated transmission properties of the photonic crystals $(ENG_1MNG_1)_{12}$, $(ENG_2MNG_2)_6$, and $(ENG_3MNG_3)_4$. These structures are typical photonic crystals structures, since they were made of two different effectively homogeneous media, ENG TL and MNG TL, so photonic band gap will exist. The center frequency in the lower frequency region is 0.57 GHz, 0.9 GHz, and 1.1 GHz, respectively, and the center frequency increase with the unit length, which is different from the conventional photonic crystals. As for the single ENG TL and MNG TL, they are opaque between 1.3 GHz and 2.1 GHz, but it is interesting that the electromagnetic wave is propagable in the periodic structures by recombining the ENG TL unit and MNG TL unit with the same TL units. For the three kinds of photonic crystals, the waves become almost completely transparent except for special gap exhibits around 1.7 GHz within the SNG gap for ENG TL and MNG TL. In the high frequency band, the conventional Bragg gaps were also observed. Figure 5(b) shows the measured S parameters, and the experimental results show a good agreement with the simulation.

Figure 6 is the simulated and measured dispersions' relation of $(ENG_1MNG_1)_{12}$ which agree well with each other. It was shown that one dimensional photonic crystal stacked by ENG TL and MNG TL can propagate electromagnetic wave. At the certain frequency $f \approx 1.76$ GHz, the effective phase shifts approach to zero, when above the frequency, propagation modes can be regarded as right-handed propagation

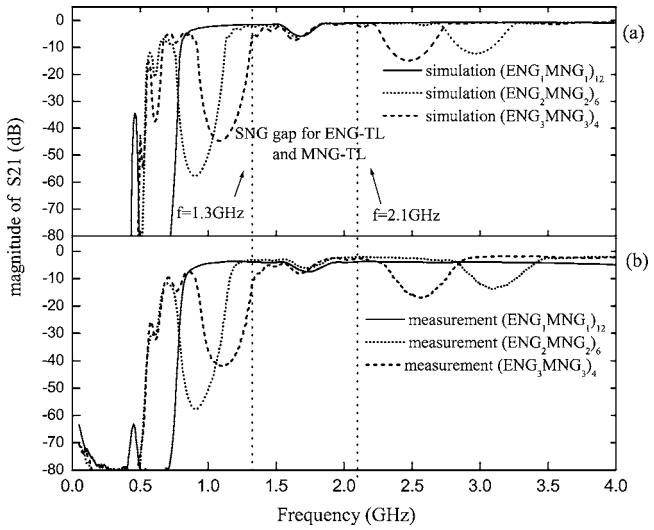

FIG. 5. The simulated (a) and measured (b) S parameters of the photonic crystals of $(ENG_1MNG_1)_{12}$, $(ENG_2MNG_2)_6$, and $(ENG_3MNG_3)_4$ based on CRLH TLs.

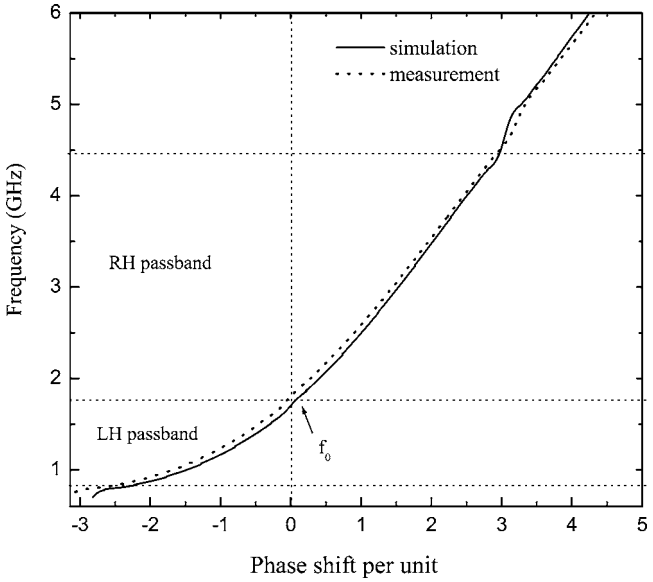

FIG. 6. The simulated and measured dispersion relations of $(\mathrm{ENG}_1\mathrm{MNG}_1)_{12}$.

modes and as left-handed propagation modes when below the frequency.

III. DISCUSSION

For the case measured above, the boundary between the left-handed propagation band and the right-handed propagation band was at $f \approx 1.76$ GHz. According to Eq. (1) based on CRLH TL, the effective relative permittivity and permeability of ENG material and MNG material can be described as

$$\epsilon_A = \epsilon_\alpha - \frac{\alpha_A}{\omega^2}, \quad \mu_A = \mu_\alpha - \frac{\beta_A}{\omega^2} \tag{3}$$

for ENG materials and

$$\epsilon_B = \epsilon_\beta - \frac{\alpha_B}{\omega^2}, \quad \mu_B = \mu_\beta - \frac{\beta_B}{\omega^2} \tag{4}$$

for MNG materials, where A and B denote ENG materials and MNG materials, respectively, ω is the angular frequency measured in GHz, $\epsilon_{\alpha(\beta)}$ and $\mu_{\alpha(\beta)}$ are constants determined by the microstrip line, $\alpha_{A(B)}$ and $\beta_{A(B)}$ are the circuit parameters that can be modulated with the loading lumped-element components series capacitors (C) and shunt inductors (L), and assuming the unit lengths are d_A and d_B, respectively. For the specific parameters used in the experimental circuit, $\epsilon_{\alpha(\beta)}=3.57$, $\alpha_A=690.9$, $\mu_{\alpha(\beta)}=1.0$, $\beta_A=87.6$, $d_A=7.2$ mm and $\alpha_B=331.6$, $\beta_B=191.9$, $d_B=8.4$ mm, respectively. First we consider a pair such as (A_nB_n), where the wave impedance $\eta_{A(B)}$ and the effective phase shift $k_{A(B)}d_{A(B)}$ in each layer can be written as

$$\eta_{A(B)} = \sqrt{|\mu_{A(B)}\mu_0/(\epsilon_{A(B)}\epsilon_0)|}, \tag{5}$$

$$k_{A(B)}d_{A(B)} = k_0\sqrt{|\epsilon_{A(B)}\mu_{A(B)}|}d_{A(B)}, \tag{6}$$

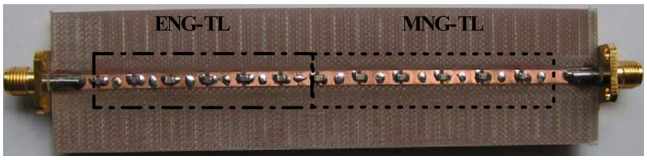

FIG. 7. (Color online) Photograph of the fabricated $(\mathrm{ENG}_6\mathrm{MNG}_6)$ pair by cascading six ENG TL units with six MNG TL units.

in its passband the refractive index in each layer can be written as

$$n_{A(B)} = \pm\sqrt{\epsilon_{A(B)}\mu_{A(B)}}, \tag{7}$$

respectively [10,18], where k_0 is the wave number in vacuum, "+" corresponds to the right-handed passband, and "–" corresponds to the left-handed passband for the refractive index, respectively. The phase-match condition $k_Ad_A = k_Bd_B$ at the wave impedance match frequency ($\eta_A = \eta_B$) decides whether the completely tunneling mode appears or not [9]. In the completely tunneling case, the energy flux will concentrate near the ENG-MNG interface where the electric field is maximum [13]. According to our circuit parameters in Eqs. (3) and (4), the phase-match frequency is close to the wave impedance-match frequency 1.89 GHz, so the electromagnetic wave can mostly propagate through the $(\mathrm{ENG}_6\mathrm{MNG}_6)$ pair at 1.89 GHz.

Figure 7 shows the $(\mathrm{ENG}_6\mathrm{MNG}_6)$ pair that was made by cascading six ENG TL units with six MNG TL units so as to investigate the tunneling phenomenon. Figure 8(a) shows the ADS simulated S parameters of the $(\mathrm{ENG}_6\mathrm{MNG}_6)$ pair using real lumped-element components that are shown in Fig. 7. It can be seen that tunneling mode occurs at $f_0=1.74$ GHz, not 1.89 GHz, which due to the difference between ideal and real lumped-element components, the insertion loss is −2.3 dB, while the return loss is −12.5 dB. Figure 8(b) shows the measured S parameters of the pair, the tunneling frequency is at $f_0=1.76$ GHz, very close to the simulated results. The in-

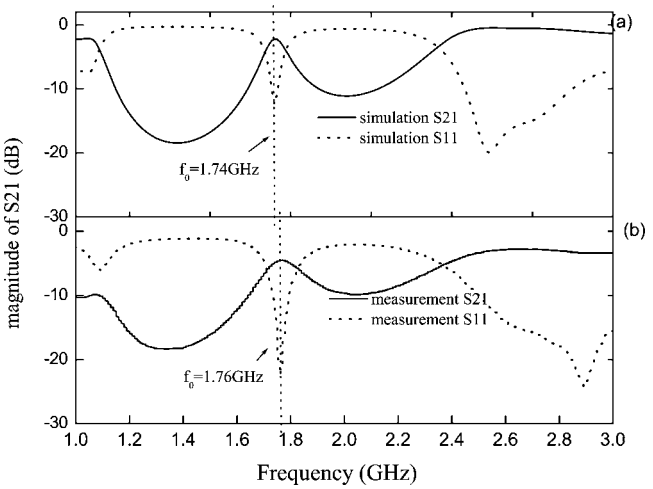

FIG. 8. The simulated (a) and measured (b) S parameters of $(\mathrm{ENG}_6\mathrm{MNG}_6)$ pair using real lumped-element components, the tunneling frequencies are 1.74 GHz and 1.76 GHz, respectively.

sertion loss and the return loss are −4.2 dB and −21 dB, respectively, with the deviations likely to come from the loss of lumped-element components and microstrip line. Compared with Fig. 6, the tunneling frequency is the transition point of left-handed propagation modes and right-handed propagation modes in photonic crystals composed of ENG materials and MNG materials.

For the Bragg gaps of the photonic crystals shown in Fig. 4, the trends of the center frequency varying with the unit length are opposite in the left-handed passband and right-handed passband for ENG TL and MNG TL, respectively, whereas the spectral gaps around 1.7 GHz are independent of the unit length in the SNG gap for ENG TL and MNG TL. In order to understand the phenomena, we consider periodic structures composed of several such $(\mathrm{ENG}_n\mathrm{MNG}_n)$ pairs in the form of $(A_3B_3)_6$, $(A_2B_2)_6$, and $(AB)_6$. First, the structures exhibit band gaps under the condition [19]

$$n_A d'_A + n_B d'_B = \frac{m\lambda_0}{2}, \tag{8}$$

where $n_{A(B)}$ is the respective refractive index and $d'_{A(B)}$ is the respective layer thickness, λ_0 is the wavelength in vacuum, and m is the band-gap index which can be any integer, including zero and negative numbers. In the condition of $m=-1$, the Bragg gaps exist in the left-handed passband for A and B. According to the dispersion characteristics, the center frequency of the gaps will increase with the thickness of each layer $d'_{A(B)}$ in the lower frequency region. When $m=+1$, the Bragg gaps appear in the right-handed passband for A and B, and the center frequency will decrease with the thickness of each layer. When $m=0$, the gaps are a new type of photonic gaps, that is zero-$\bar{n}$ gaps [20,21]. They are invariant upon the scaling, and insensitive to the disorder and incident angle of incident wave which is distinct from conventional Bragg gaps. But the condition of $\bar{n}=0$ is not fulfilled here, because the ENG material and MNG material described in Figs. 2(a) and 2(b) have the same sign of refractive index in the same frequency band. Jiang *et al.* [10] and Wang *et al.* [22] found that the periodic structure composed of ENG materials and MNG materials can possess the zero effective phase (zero-Φ_{eff}) gaps. They are another type of photonic gaps that are also insensitive to the incident angle and the wave polarizations, invariant upon the changes of scale length. The important feature of the zero-Φ_{eff} gaps is that they are surrounded by propagation modes. The propagation modes are the left-handed propagation modes and the right-handed propagation modes, respectively, because of the interaction of the evanescent-wave-based interface modes in each period which can be explained with the aid of a tight-binding model in solid-state physics [8,10].

Figures 9(a), 9(b), and 9(c) show the transmission of $(A_3B_3)_4$, $(A_2B_2)_6$, and $(AB)_{12}$ structures calculated with the help of transfer matrix [18,23], respectively. When $m=-1$, the center frequencies of the Bragg gaps are about 0.55 GHz, 0.95 GHz, and 1.16 GHz for $(AB)_{12}$, $(A_2B_2)_6$, and $(A_3B_3)_4$, respectively, increasing with the thickness of each layer which is different from that of $m=1$ in the high frequency band. Between the frequencies 1.53 GHz–2.2 GHz, the evanescent wave for both A and B become the propagation wave in the three kinds of periodic structures. The propagation characteristics of the periodic structures composed of A and B are very similar to that in the left-handed materials or right-handed materials, which are determined by the average permittivity $[\bar{\epsilon}=(\epsilon_A d'_A+\epsilon_B d'_B)/(d'_A+d'_B)]$ and average permeability $[\bar{\mu}=(\mu_A d'_A+\mu_B d'_B)/(d'_A+d'_B)]$. The frequency where $\bar{\epsilon}=0$ and $\bar{\mu}=0$ is completely tunneling frequency, then the tunneling mode is a transmission point from the left-handed propagation modes to the right-handed propagation modes. Figure 9(d) shows the calculated $\bar{\epsilon}$ and $\bar{\mu}$ of $(AB)_{12}$; $\bar{\epsilon}$ and $\bar{\mu}$ equal zero at 1.88 GHz and 1.91 GHz, respectively, and $\bar{\epsilon}$ and $\bar{\mu}$ are both negative when frequency $f<1.88$ GHz and positive when $f>1.91$ GHz. The photonic crystals can be regarded as an SNG material between the narrow frequency regions 1.88–1.91 GHz, where the zero-Φ_{eff} gaps exist, which is insensitive to the thickness symmetric fluctuation of pair layers. The spectral gaps of the three kinds of photonic crystals stay almost at the same frequency region shown in Figs. 9(a)–9(c). Therefore, the shallow gaps in the three kinds of photonic crystals shown in Fig. 5 are zero-Φ_{eff} gaps.

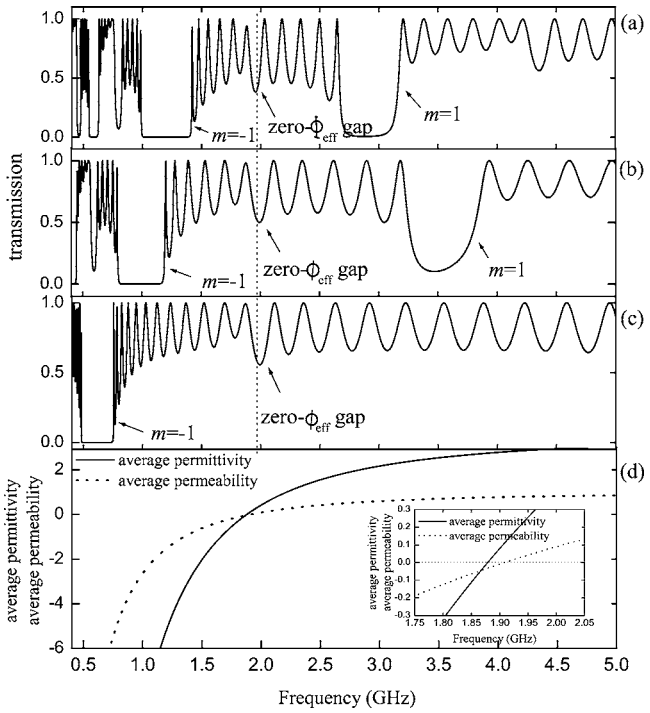

FIG. 9. The calculated transmission of the photonic crystals $(A_3B_3)_4$ (a), $(A_2B_2)_6$ (b), $(AB)_{12}$ (c), where m is the band-gap index, (d) shows the average permittivity $(\bar{\epsilon})$ and the average permeability $(\bar{\mu})$ of photonic crystals, and the inset illustrates the partial average permittivity and average permeability vs frequency from 1.75 GHz–2.05 GHz.

IV. CONCLUSION

ϵ-negative (ENG) and μ-negative (MNG) materials are successfully fabricated by using composite right/left-handed transmission line (CRLH TL), which are opaque in experiments. We experimentally demonstrate the tunneling phe-

nomenon occurring in the ENG-MNG pair, and verified that left-handed material can be realized by stacking ENG and MNG materials in experiments. The photonic crystals consisting of ENG materials and MNG materials based on CRLH TL can possess left-handed propagation mode and right-handed propagation mode within forbidden gaps. It is theoretically show that the interactions of the evanescent-wave-based interface modes contribute to the unusual properties. At the same time, the Bragg gap for the band-gap indices $m=\pm 1$ and the zero-Φ_{eff} gaps were also observed. The experimental results agree extremely well with the simulations.

ACKNOWLEDGMENTS

This research was supported by National Basic Program (973) of China (Grant No. 2006CB0L0901) and by the National Natural Science Foundation of China (Grant Nos. 50477048 and 10474072).

[1] V. G. Veselago, Sov. Phys. Usp. **10**, 509 (1968).
[2] R. A. Shelby, D. R. Smith, and S. Schultz, Science **292**, 77 (2001).
[3] D. R. Smith, W. J. Padilla, D. C. Vier, S. C. Nemat-Nasser, and S. Schultz, Phys. Rev. Lett. **84**, 4184 (2000).
[4] G. V. Eleftheriades, O. Siddiqui, and A. K. Iyer, IEEE Microw. Wirel. Compon. Lett. **13**, 51 (2003).
[5] C. Caloz and T. Itoh, IEEE Trans. Antennas Propag. **52**, 1159 (2004).
[6] M. A. Antoniades and G V. Eleftheriades, IEEE Antennas Wireless Propag. Lett. **2**, 103 (2003).
[7] C. Caloz, Atsushi Sanada, and T. Itoh, IEEE Trans. Microwave Theory Tech. **52**, 980 (2004).
[8] D. R. Fredkin and A. Ron, Appl. Phys. Lett. **81**, 1753 (2002).
[9] A. Alù and N. Engheta, IEEE Trans. Antennas Propag. **51**, 2558 (2003).
[10] H. T. Jiang, H. Chen, H. Q. Li, Y. W. Zhang, J. Zi, and S. Y. Zhu, Phys. Rev. E **69**, 066607 (2004).
[11] J. B. Pendry, A. J. Holden, W. J. Stewart, and I. Youngs, Phys. Rev. Lett. **76**, 4773 (1996).
[12] J. B. Pendry, A. J. Holden, D. J. Robbins, and W. J. Stewart, IEEE Trans. Microwave Theory Tech. **47**, 2075 (1999).
[13] T. Fujishige, C. Caloz, and T. Itoh, Microwave Opt. Technol. Lett. **46**, 476 (2005).
[14] G. S. Guan, H. T. Jiang, H. Q. Li, Y. W. Zhang, and H. Chen, Appl. Phys. Lett. **88**, 211112 (2006).
[15] C. Caloz, A. Lai, and T. Itoh, New J. Phys. **7**, 167 (2005).
[16] A. Grbic and G. V. Eleftheriades, J. Appl. Phys. **92**, 5930 (2002).
[17] J. S. Hong and M. J. Lancaster, *Microstrip Filters for RF/Microwave Application* (Wiley, New York, 2001).
[18] H. T. Jiang, H. Chen, H. Q. Li, Y. W. Zhang, and S. Y. Zhu, J. Appl. Phys. **98**, 013101 (2005).
[19] M. W. Feise, I. V. Shadrivov, and Y. S. Kivshar, Appl. Phys. Lett. **85**, 1451 (2004).
[20] J. Li, L. Zhou, C. T. Chan, and P. Sheng, Phys. Rev. Lett. **90**, 083901 (2003).
[21] H. T. Jiang, H. Chen, H. Q. Li, Y. W. Zhang, and S. Y. Zhu, Appl. Phys. Lett. **83**, 5386 (2003).
[22] L. G. Wang, H. Chen, and S. Y. Zhu, Phys. Rev. B **70**, 245102 (2004).
[23] N. H. Liu, S. Y. Zhu, H. Chen, and X. Wu, Phys. Rev. E **65**, 046607 (2002).